ELSEVIER

Biophysical Chemistry 64 (1997) 139–155

Biophysical Chemistry

Competitive electrostatic binding of charged ligands to polyelectrolytes: practical approach using the non-linear Poisson–Boltzmann equation

Ioulia Rouzina, Victor A. Bloomfield *

Department of Biochemistry, University of Minnesota, 1479 Gortner Avenue, St. Paul, MN 55108, USA

Received 22 July 1996; revised 15 August 1996; accepted 15 August 1996

Abstract

We have developed a practical analytical treatment of the non-linear Poisson–Boltzmann (P–B) equation to characterize the strong but non-specific binding of charged ligands to DNA and other highly charged macromolecules. These reactions are notable for their strong salt dependence and anti-cooperativity, features which the theory fully explains. We summarize analytical results for concentration profiles and ion binding in various regimes of surface curvature and ionic strength, and show how counterion size and charge distribution may influence competitive binding. We present several practical applications of the formalism, showing how to estimate the ligand concentration needed to effectively compete with a given buffer salt, and how to calculate the amounts of counterion species bound at various distances from the DNA surface under given bulk solution conditions. We cast our results into the form of a Scatchard binding isotherm, showing how the apparent binding constant K_{obs} and $S = -\mathrm{d}\log K_{obs}/\mathrm{d}\log[M^+]$ can be predicted from the basic theory. Anti-cooperativity arises naturally without steric repulsion, and binding curves can be fitted with K_{obs} and effective charge as the only free parameters. We extend the analytical P–B analysis to an arbitrary number of counterion species, and apply the results to fit and predict three-ion competition data.

Keywords: Charged ligands; Competitive electrostatic binding; Non-linear Poisson–Boltzmann equation; Polyelectrolytes

1. Introduction

An important class of reactions in biology is the strong but non-specific binding of charged ligands to DNA and other highly charged macromolecules. These reactions have two common characteristics. First, the binding is generally strongly salt-dependent. If, as is common, the reaction is written as a chemical equilibrium with one ligand molecule L releasing S salt counterions M^+ upon its binding to DNA [1]

$$\mathrm{DNA} + \mathrm{L}^{S+} \rightleftharpoons \mathrm{DNAL} + S\,\mathrm{M}^+ \quad (1)$$

$$K_{obs} = \frac{[\mathrm{DNAL}]}{[\mathrm{DNA}][\mathrm{L}]} = \frac{K}{[\mathrm{M}^+]^S} \quad (2)$$

the apparent binding constant K_{obs} decreases according to the power S of the salt concentration

$$S = -\frac{\mathrm{d}\log K_{obs}}{\mathrm{d}\log[\mathrm{M}^+]} \approx \frac{z_2}{z_1} \quad (3)$$

* Corresponding author. Tel.: (612) 625-2268; fax.: (612) 625-6775; e-mail: victor@biosci.cbs.umn.edu

PII S0301-4622(96)02231-4

where z_1 and z_2 are the charges of the salt and ligand, respectively.

Second, these reactions are often highly anti-cooperative: the apparent binding constant decreases strongly as the fractional degree of ligand binding Θ_2 increases. The anti-cooperativity is often treated as a steric repulsion between the ligands, each occluding N consecutive sites upon its binding to the linear array of polymer binding sites, according to the familiar McGhee–von Hippel binding isotherm [2]

$$\frac{\Theta_2}{[\mathrm{L}]} = K_{\mathrm{obs}} \frac{(1 - N\Theta_2)^N}{[1 - (N-1)\Theta_2]^{N-1}} \tag{4}$$

where K_{obs} is now the apparent binding constant in the limit of zero binding. The two parameters K_{obs} and N are usually sufficient to fit any binding data.

However, this common approach has a number of unsatisfactory practical and conceptual deficiencies. For example, the apparent site size N in most cases increases with z_2/z_1; however the source of this relationship is unclear, since the meaning of N in Eq. (4) is the physical size rather than the charge of the ligand. Fitting binding data for the same ligand at various salt concentrations often yields N values which vary randomly by up to 50%, but with a general tendency to decrease in higher salt concentrations.

At a more fundamental level, the appropriateness for non-specific binding of the chemical reaction model embodied in Eq. (1) is open to question. The strong salt dependence, together with typically very low values of K_{obs} at salt concentrations about 1 M or above, suggest that the main driving force for binding is the purely electrostatic, non-specific association of the ligand with the macroion. Both experimental [3–7] and theoretical [8–14] studies have established convincingly that ions are attracted to the DNA surface as a whole, rather than to individual phosphates. This behavior is especially emphasized in counterion condensation theory [15]. In other words, the ions are not localized electrostatically at certain sites on the DNA but are essentially free to move along its surface in any direction, except for a slight preference for the grooves which vanishes for ions larger than 2 Å radius [14,16].

The steric repulsion between counterions in such a mobile charge cloud is negligible even for quite large ions [17]. For example, B-DNA has about a 100 Å^2 surface area per unit charge. Therefore, even at the highest counterion concentrations with all ions at the surface, the average distance between two monovalent counterions is about 10 Å. For higher valence counterions, the average distance is even larger: $10\sqrt{z_2}$ Å. The electrostatic repulsion between the ions keeps them as far as possible from each other, so that ions as large as 10–15 Å do not experience significant steric repulsion. Thus the explanation of anti-cooperativity by physical occlusion of localized sites on a linear polyelectrolyte seems inconsistent with the underlying physics of electrostatic binding, a point made earlier by Ray and Manning [18].

The conventional model of an ion exchange reaction with fixed stoichiometry is inappropriate to describe purely electrostatic ligand binding for another reason. Both ligand and buffer ions have a continuous distribution of free energy within the screening counterion cloud. Therefore, there is no single value for the free energy of ion binding that would lead to an exchange reaction with fixed stoichiometry.

Given these inadequacies of the conventional model, a new approach seems desirable. Such an approach should employ a more realistic physical picture of non-specific electrostatic binding, enabling the derivation of all observed features including the values of N and K_{obs} directly from electrostatics without postulating any poorly defined "binding sites". On the other hand, such a new approach should also be simple enough that it can be readily applied to practical situations, without elaborate calculations.

In this paper, we show how a practical approach to non-specific electrostatic ligand binding can be developed using the non-linear Poisson–Boltzmann (P–B) equation. This is an extension of our previous work [19,20], summarizing and clarifying the theoretical development and showing how the key equations can be applied to a variety of experimentally important situations.

The screening of a charged surface by a mixture of counterions is conceptually simple, and has been treated by a large variety of statistical mechanical theories, most of which must be solved numerically to yield useful results. The simplest theory of poly-

electrolyte solutions that provides a level of structural detail adequate for our purposes is embodied in the P–B equation [9–13,21–27]. The ligand may be represented as a hard sphere or point charge, or with a detailed geometry and partial charge distribution. The DNA double helix may also be modeled at different levels of structural detail, but its electrostatic properties are well represented by a uniformly charged cylinder [9,11,14,28]. The main features of competitive ligand binding are often adequately captured by the simplest geometry: two hard spheres of different charge and size, near a uniformly charged cylinder [10,20]. Strikingly, as we shall see below, this model can be further simplified to ion competition near a planar charged wall.

Using the non-linear P–B approximation, however, has in the past involved numerical solution of the differential equation followed by integration of the excess ion concentration profile to obtain the amount of ligand bound at any particular condition. This procedure is not simple enough to predict general trends and make practical estimates of binding parameters. In our preceding papers [19,20], we developed an approximate (but simple, explicit, and reasonably accurate) analytical description of counterion competition near an arbitrarily curved surface with any charge density in a solution of any ionic strength. In this paper, we summarize and apply this approach to a variety of problems relevant to the competitive binding of charged ligands to DNA. The results are also applicable to other highly charged macromolecules.

In Section 2 we summarize analytical results for concentration profiles and ion binding in various regimes of surface curvature and ionic strength, and in Section 3 show how counterion size and charge distribution may influence competitive binding. In Section 4 we present several practical applications of the formalism, showing how to estimate the ligand concentration needed to effectively compete with a given buffer salt, and how to calculate the amounts of counterion species bound at various distances from the DNA surface under given bulk solution conditions.

In Section 5 we cast our results into the form of a Scatchard binding isotherm, showing how the parameters K_{obs} and S can be predicted from the basic theory. Anti-cooperativity arises naturally without steric repulsion, and binding curves can be fitted with K_{obs} and effective charge as the only free parameters. In Section 6, we extend the analytical P–B analysis to an arbitrary number of counterion species, and apply the results to fit and predict three-ion competition data. Finally, in Section 7 we summarize our results.

2. Summary of theoretical results

In this section and the next we summarize the main results obtained in our earlier papers [19,20], and introduce some correction factors that yield better agreement with exact numerical solutions. In the first of those papers, we showed that the non-linear P–B equation could be solved analytically in different regimes, depending on the relative magnitudes of three characteristic lengths: the radius of curvature R of the polyion surface, the Debye screening length r_d, and the decay length λ_z of the distribution of z-valent counterions at the polyion surface. For highly charged polyions like DNA, to which we confine our attention in this paper, λ_z is always less than R and r_d. When $R > r_d$, at high ionic strength, the DNA can be treated as if it is a planar surface; when $R < r_d$, at low ionic strength, the DNA must be treated as a cylinder. The following quantities are the same in any geometry

$$\text{Bjerrum length: } l_b = \frac{q_e^2}{\varepsilon k_B T} \tag{5}$$

$$\text{Surface charge density: } \sigma = \frac{q_e}{2\pi b R} \tag{6}$$

$$\text{Thickness of counterion layer: } \lambda_z = \frac{q_e}{4\pi\sigma l_b z} \tag{7}$$

$$\text{Ionic strength: } I = \frac{1}{2}\sum_i n_{bi} z_i^2 \tag{8}$$

$$\text{Debye screening length: } r_d = (8\pi I l_b)^{-1/2} \tag{9}$$

$$\text{Manning ratio: } \xi = l_b/b \tag{10}$$

where q_e is the elementary charge, ε is the dielectric constant, k_B is the Boltzmann constant, T is the temperature, b is the charge spacing along the DNA helix, and n_{bi} is the bulk molar concentration of the

ith ion of charge z_i. In water at 25°C, $l_b = 7.14$ Å and $r_d = 3.3/\sqrt{I}$ Å. For B-DNA with $b = 1.69$ Å and $R = 10$ Å, $\sigma = 4.5 \times 10^4$ esu cm^{-2}, corresponding to one charge per 106 Å^2; $\lambda_z = 1.19$, 0.595, and 0.397 Å for $z = 1$, 2, and 3 respectively; and $\xi = 4.2$. The values of σ and λ_z are for point charges. All distances should be measured from the distance of closest approach to the polyion surface (Fig. 1). This has the effect of increasing the effective R, reducing σ, and changing proportionately all quantities that depend on these.

2.1. Single counterion near a highly charged surface

Although our main interest is in the competition between different counterion species, we must first understand the behavior of single species of counterion interacting with highly charged (effectively) planar and cylindrical surfaces.

2.1.1. Planar surface

A key quantity is the surface concentration of counterions n_s, which for a plane is

$$n_s = 2\pi(\sigma/q_e)^2 l_b \tag{11}$$

Analytical solution of the P–B equation near a highly charged planar surface with a single counterion species yields the excess counterion concentration $\Delta n(r) = n(r) - n_b$ at distances $r < r_d$ from the surface

$$\Delta n(r) = \frac{n_s}{(1 + r/2\lambda_z)^2} \tag{12}$$

For B-DNA, the surface counterion concentration is very high: $n_s = 6.65$ M. The non-linear counterion distribution described by Eq. (12) exists only for a highly charged surface and sufficiently low ionic strength: $\lambda_z \ll r_d$ or, equivalently, $I \ll n_s$. For B-DNA, this requires $I < 1$ M, not a very severe limitation. For ions of finite size, r is the distance from the surface to the ion center.

The ion distribution Eq. (12) is independent of the bulk solution. The thin "condensed" layer of counterions does not dissolve even at infinite dilution. This is the P–B analog of counterion condensation [15] with a volume per condensed ion of approximately $\lambda_z bR$. However, in contrast to the analogous quantity V_p in counterion condensation theory, $\lambda_z bR$ decreases with increasing z and decreasing T or ε, in better accord with physical intuition.

The fraction of charge $z\Theta(r)$ neutralized by counterions within a distance r from the surface is found by integrating Eq. (12) and noting that $2zq_e n_s \lambda z/\sigma = 1$

$$z\Theta(r) = g\left(\frac{r}{\lambda_z}\right) = \frac{zq_e}{\sigma}\int_0^r dr'\Delta n(r') = 1 - \frac{1}{1 + \dfrac{r}{2\lambda_z}} \tag{13}$$

where we have combined Eq. (5)–(7) to show that

$$2zq_e n_s \lambda_z/\sigma = 1 \tag{14}$$

A considerable fraction of the surface charge is neutralized within a few λ_z, one-half within $2\lambda_z$. Eq. (14) shows that a simple estimate of the fractional charge bound as a product of the counterion charge density at the surface $zq_e n_s$ and the thickness λ_z yields a quantity close to the full surface charge σ.

The salt independent part of the excess counterion profile (Eq. (12)) holds up to distances $r \approx r_d$ from the surface. The remaining part of the surface charge

$$1 - g\left(\frac{r_d}{\lambda_z}\right) \simeq \left(\frac{4I}{z^2 n_s}\right)^{1/2} \tag{15}$$

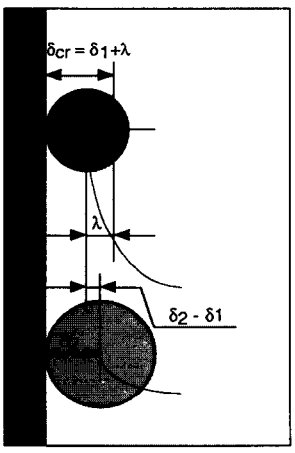

Fig. 1. Two counterion species binding to and screening a highly charged surface. See text for definition of symbols.

is screened within the Debye–Hückel exponential tail, and is not described by Eq. (13).

2.2. Cylindrical surface

When the radius of curvature is less than the Debye length

$$\frac{R}{r_d} = \sqrt{\frac{4\xi^2 I}{n_s}} < 1 \tag{16}$$

the cylindrical P–B equation must be used. For B-DNA, Eq. (16) shows that this occurs at $I \leq 0.1$ M. However, if the polyion charge density is still so high that

$$\frac{R}{2\lambda_z} = z\xi > 1 \tag{17}$$

which corresponds to the condition for counterion condensation [15], then screening is similar to the planar regime.

Solution of the P–B equation with a single counterion species in cylindrical geometry leads to the renormalized excess surface concentration

$$n_s^* = n_s(1 - 1/z\xi)^2 \tag{18}$$

and the excess concentration profile

$$\Delta n(r) = \frac{n_s^*}{\left[1 + (z\xi - 1)\ln\left(\frac{R+r}{R}\right)\right]^2}\left(\frac{R}{R+r}\right)^2 \tag{19}$$

The n_s^* value is not very different from the planar value n_s if $z\xi \gg 1$, i.e. the cylinder is highly charged.

Expansion of Eq. (19) with respect to r/R yields the standard decay length λ_z near the surface, since this is fixed by σ. Integration of $\Delta n(r)$ yields

$$z\Theta(r) = zq_e\int_R^r d^3r'\Delta n(r') = zq_e + \frac{R}{z\xi - 1}\left[1 - \frac{1}{1 + (z\xi - 1)\ln\left(\frac{R+r}{R}\right)}\right] \tag{20}$$

which for $r \ll R$ can be written as

$$z\Theta(r) = \frac{zq_e n_s^* 2\lambda_z^*}{\sigma}\left(1 - \frac{1}{1 + \frac{r}{2\lambda_z^*}}\right) \tag{21}$$

Here we used Eq. (17) and introduced the quasi-planar decay length

$$\lambda_z^* = \lambda_z/(1 - 1/z\xi) \tag{22}$$

It follows from Eq. (14) and (21) that the maximum fraction of charge which can be neutralized within the non-linear (independent of the bulk salt) part of the counterion distribution is

$$\frac{2zq_e n_s^* \lambda_z^*}{\sigma} = 1 - 1/z\xi \tag{23}$$

Comparing Eq. (21) and (13), we can write the fraction of charge bound to the cylinder as

$$z\Theta(r) = (1 - 1/z\xi)\, g\left(\frac{r}{\lambda_z^*}\right) \tag{24}$$

At any finite salt concentration, the remaining $1 - z\Theta > 1 - 1/z\xi$ charge will be neutralized on the scale of r_d.

2.3. Competition between two counterion species

If the solution contains two or more counterion species, the excess concentration profile for each of them is similar to Eq. (12) or (19), depending on the effective geometry. This is because the decay length λ_z for each species is independent of the presence of the others; the physical significance of λ_z is the average distance of the ion with thermal energy $k_B T$ to the highly charged surface attracting it with an electrostatic field $E_0 = 4\pi\sigma/\varepsilon$. However, the surface concentration n_s in Eq. (12) or n_s^* in Eq. (19) should be replaced by the surface concentrations n_{si} or n_{si}^* for each species. These are not independent, and the relationship between the surface ionic concentrations depends on the geometry of the surface. In this section we consider just two competing counterions; more than two will be treated in Section 6.

2.3.1. Counterion competition near a charged plane

The surface boundary condition for the planar P–B equation requires

$$n_{s1} + n_{s2} = n_s \tag{25}$$

This equation, together with the Boltzmann law at the surface

$$n_{s1} = n_{b1} e^{z_1 \Psi_s} \text{ and } n_{s2} = n_{b2} e^{z_2 \Psi_s} \tag{26}$$

fully determines the surface concentrations (n_{s1}, n_{s2}) in terms of the bulk concentrations (n_{b1}, n_{b2}) and the surface electrostatics (n_s). Eliminating the reduced surface potential $\Psi_s = -q_e \phi_s / k_B T$ (ϕ is the actual potential) from Eq. (26) yields

$$\frac{\tilde{n}_{s2}}{(\tilde{n}_{s1})^{z_2/z_1}} = Y \text{ and } \tilde{n}_{s1} = 1 - \tilde{n}_{s2} \tag{27}$$

where

$$Y = \frac{n_{b2}}{n_{b1}^{z_2/z_1}} n_s^{z_2/z_1 - 1} \tag{28}$$

and

$$\tilde{n}_{si} = n_{si}/n_s \tag{29}$$

is the fractional surface concentration of the ith species which varies from 0 to 1 upon titration of the solution with this counterion. The dependence of $\tilde{n}_{si}$ on log Y for the competition of monovalent counterions with di-, tri-, tetra- and pentavalent competitors is shown in Fig. 2.

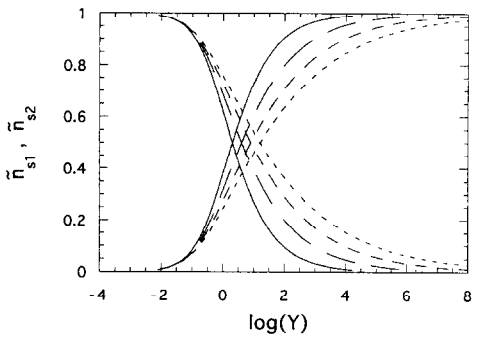

Fig. 2. Reduced surface concentration $\tilde{n}_{si} = n_{si}/n_s$ for two competing species as a function of the bulk solution composition and the surface electrostatics represented by parameter Y, Eq. (28), for planar geometry. The parameter Y increases with increasing relative n_{b2}. Species 1 is monovalent, and is represented by the curves that decrease with increasing Y. Species 2 has valence 2, 3, 4 and 5, with shorter dashes corresponding to the higher valences, and is represented by the curves that increase with increasing Y.

Knowing the individual concentration profiles, Eq. (12), and n_{si} and λ_{zi} we can calculate the amounts of each species bound at any bulk composition (n_{b1}, n_{b2})

$$z_i \Theta_i(r) = \tilde{n}_{si}\, g\left(\frac{r}{\lambda_{zi}}\right) \tag{30}$$

This is the main result of our approach. It quantifies the dependence of the amount of each species bound on the bulk composition and surface electrostatics combined in parameter Y, through the reduced surface concentrations $\tilde{n}_{si}(Y)$. These can be found from Eq. (27) without solving the P–B equation. The dependence of the bound charge on the distance from the surface is contained in the $g(r/\lambda_{zi})$ function, Eq. (13). Note that this function will be larger for the higher valent species since the thickness of the counterion layer is inversely proportional to the counterion charge.

The accuracy of this approach is examined in Fig. 3, which compares the fraction of screening charge due to each species within the cut-off distance r_{cut}, $z_i \Theta_i(r_{cut})$, as calculated by the approximate Eq. (30) and by numerical solution of the P–B equation. Note that the $g(r_{cut}/\lambda_{zi})$ factor will be larger for higher valent species since the thickness λ_z of the counterion layer is inversely proportional to the counterion charge. The approximation is very good for short cut-off distances ($r_{cut} \approx \lambda_z$), and gets worse for larger r_{cut} but is still reasonable even at $r_{cut} \to \infty$. This becomes especially evident in Fig. 4 where $z_i \Theta_i(\infty)$, with n_{b1} for monovalent cations ranging from 10^{-4} to 10^{-1} M and n_{b2} for trivalent cations from 10^{-16} to 10^{-2} M, is plotted vs. Y. The $z_i \Theta_i(\infty)$ curves are close to each other and to the $\tilde{n}_{si}$. It is also evident that the accuracy of Eq. (30) for $r_{cut} \to \infty$ gets better at higher solution ionic strength. This is a little unexpected, since the accuracy of the approximation is certainly limited by the requirement $I \ll n_s$

$$\text{err}_1 \simeq \left(\frac{I}{n_s}\right)^{1/2} \tag{31}$$

In general, one can say that Eq. (30) is adequate for the higher-valent counterion, and that Eq. (30) should have a term of order err_1 added to it to

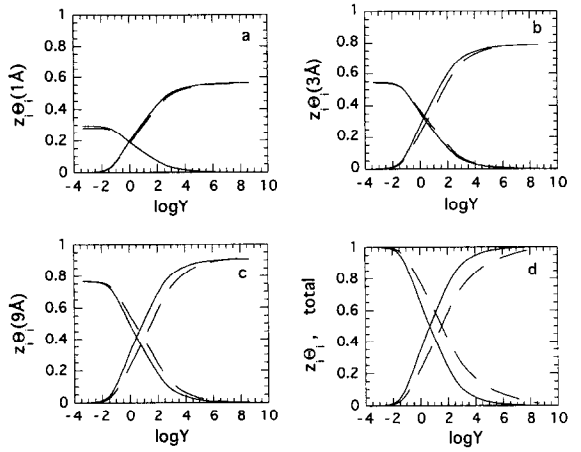

Fig. 3. The fraction of the planar surface charge $z_i\Theta_i(r_{cut})$ screened by competing monovalent ($i = 1$, decreasing left to right) and trivalent ($i = 2$, increasing left to right) ions as a function of the bulk composition variable Y, Eq. (28). The bulk monovalent ion concentration n_{b1} was fixed at 10^{-4} M, and Y was varied by increasing n_{b2}. The cut-off radii r_{cut} for charge integration are (a) 1 Å, (b) 3 Å, (c) 9 Å, and (d) ∞. The surface charge density was that of B-DNA, and the counterions were treated as point charges. The broken lines are from numerical integration of the planar P–B equation; the solid lines are from Eq. (30).

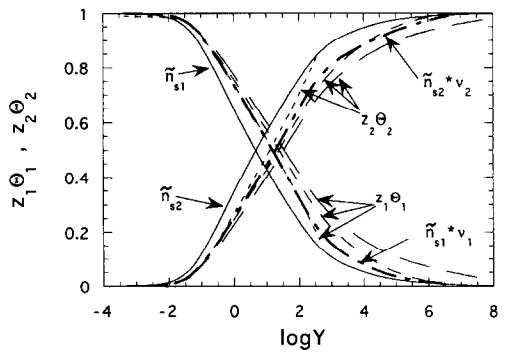

Fig. 4. The total fraction of the planar surface charge $z_i\Theta_i(\infty)$ screened by monovalent and trivalent competing species as a function of the bulk composition represented by Y. The dashed lines are from numerical integration of the P–B equation for the plane. The thin solid lines are the corresponding reduced surface concentrations $\tilde{n}_{si}$, which serve as a first approximation to all the numerical dependences. The bold dash–dotted lines are the improved approximation $z_i\Theta_i(\infty) = \tilde{n}_{si}\nu_i$, Eq. (32). In each calculation, the monovalent ion concentration was fixed at 10^{-4}, 10^{-2} or 10^{-1} M, while the trivalent counterion concentration was varied; the longer dashes correspond to lower ionic strength.

account for the screening by the lower-valent counterion in the region $r > r_d$.

However, for two competing species there is another source of inaccuracy: the deviation of each excess counterion profile from Eq. (12) upon titration. This deviation is negligible close to the surface ($r = \lambda_z$) where the decay of each concentration profile is defined by the unscreened surface field. It becomes somewhat larger at longer distances, as seen in Fig. 3 of our previous paper [19]. Being minor, but integrated up to a large distance of approximately $r_d \gg \lambda_z$, this deviation can significantly alter the accumulated charge from its estimate in Eq. (30). This can be improved to some extent by introducing correction factors ν_1 and ν_2 into Eq. (30) for large cut-offs $r_{cut} > r_d$

$$z_i\Theta_i(\infty) = \tilde{n}_{si}\nu_i \tag{32}$$

where

$$\nu_1 = \frac{1}{1-(1-z_1/z_2)/(2-z_1/z_2)\tilde{n}_{s2}} \text{ and}$$

$$\nu_2 = \frac{1}{2-z_1/z_2-(1-z_1/z_2)\tilde{n}_{s2}} \tag{33}$$

correct for the slight changes in the shape of the excess concentration profile of each species upon titration. These factors were obtained by interpolation between their values in the two limiting cases $z_1\Theta_1 \to 0$ and $z_2\Theta_2 \to 0$. The limiting value of $\nu_2(z_2\Theta_2 \to 0)$ can be calculated by analytically integrating the excess concentration of the second species in the potential for screening by the first species only, which we know from the single species profile, Eq. (12); and visa versa for $\nu_1(z_1\Theta_1 \to 0)$. The two factors are related throughout the titration by $\tilde{n}_{s1}\nu_1 + \tilde{n}_{s2}\nu_2 = 1$.

As can be seen in Fig. 4, these factors indeed correct for the major salt-independent part of the error. The remaining error is largest when the higher valent species is in a majority at the surface. This is because strong screening of the surface at very short distances of around $\lambda_{z2} < \lambda_{z1}$ slows down the decay of the lower valent species distribution. However, this is always less than

$$\text{err}_2 = 0.01(n_s/I)^{(1/2-z_1/z_2)} \tag{34}$$

When applying Eq. (30), $z_1\Theta_1$ should be increased by an amount of order err_2, and $z_2\Theta_2$ should be decreased by a similar amount. For 0.01 M ionic strength with trivalent and monovalent counterions, the error in $z\Theta(\infty)$ is always less then 3%. The err_2 becomes larger at lower ionic strength and for more asymmetric charges of the counterion species, as illustrated in Fig. 5. We see that in the last panel, where $(1/2 - z_1/z_2) < 0$, even very low salt concentration yields a rather high accuracy.

The err_1 and err_2 are additive, and suggest that the accuracy of Eq. (32) gets worse for too low as well as for too high ionic strengths. However, the total error is still less than 15% for ionic strengths in the wide range 10^{-5} M $< I <$ 0.1 M. Eq. (32) is most accurate at intermediate I values of about 0.001–0.01 M. The importance of the approximate Eq. (30) and (32) is that they combine reasonable accuracy with great simplicity. They should be used for $r_{cut} < r_d$ and $r_{cut} > r_d$, respectively.

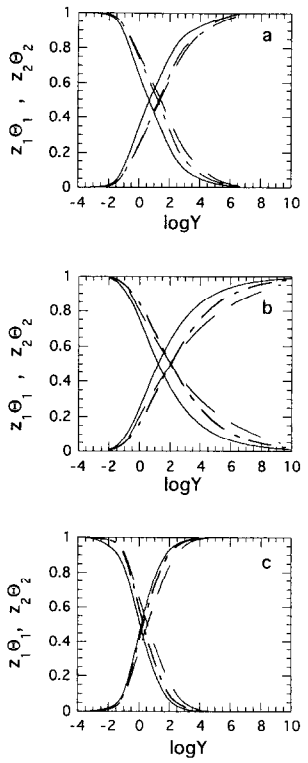

Fig. 5. The same as Fig. 4, but for different pairs of ion charges. The curves are for a specific value of the bulk concentration of the lower-valent species and varying concentration of the higher-valent species. The dashed lines are numerical P–B results, the solid lines are reduced surface concentrations $\tilde{n}_{si}$, and the dash–dotted lines are $\tilde{n}_{si}\nu_i$ values. The concentrations and valence pairs are (a) $n_{b1} = 10^{-2}$ M, $z_1 = 1$, $z_2 = 3$; (b) $n_{b1} = 10^{-2}$ M, $z_1 = 1$, $z_2 = 5$; (c) $n_{b1} = 10^{-5}$ M, $z_1 = 2$, $z_2 = 3$.

2.3.2. Counterion competition near a charged cylinder

Considering the character of the single counterion species distribution around a cylinder, we can easily extend most of the above conclusions with respect to species competition to the cylindrical case. One cannot write the exact equality of Eq. (25) for cylindrical geometry, but in practice a very similar relationship holds

$$\frac{n_{s1}}{n_s(1 - 1/z_1\xi)^2} + \frac{n_{s2}}{n_s(1 - 1/z_2\xi)2} = 1 \qquad (35)$$

where the two terms are the surface concentrations of species 1 and 2 reduced by their maximum values n^*_{si}: $\tilde{n}_{si} = n_{si}/n^*_{si}$, where n^*_{si} are defined by Eq. (18).

As in the planar case, the variation of $\tilde{n}_{si}$ from 0 to 1 with the bulk composition follows the titration. Eq. (26) and (35) allow the calculation of $\tilde{n}_{si}$ without solving the P–B equation. It is the same function of composition for the cylinder as for the plane, but of the slightly different parameter Y^*:

$$\frac{\tilde{n}^*_{s2}}{(\tilde{n}^*_{s1})^{z_2/z_1}} = Y^* \text{ and } \tilde{n}^*_{s1} = 1 - \tilde{n}^*_{s2} \qquad (36)$$

$$Y^* = Y\chi, \quad \chi = \left[\frac{(1 - 1/z_1\xi)^{z_2/z_1}}{1 - 1/z_2\xi}\right]^2 \qquad (37)$$

This, in turn, yields the amount of charge neutralization as a function of distance from the cylinder

$$z_i\Theta_i(r) = \tilde{n}^*_{si}\, g(r/\lambda^*_{zi})(1 - 1/z_i\xi), \quad r < r_d \qquad (38)$$

and

$$z_1\Theta_1(\infty) = \tilde{n}^*_{s1}(1 - 1/z_1\xi)\nu_1 + [1 - (z_1\Theta_1 + z_1\Theta_2)],$$
$$z_2\Theta_2(\infty) = \tilde{n}^*_{s2}(1 - 1/z_2\xi)\nu_2, \quad r \gg r_d \qquad (39)$$

These equations are compared with numerical solutions to the cylindrical P–B equation in Fig. 6.

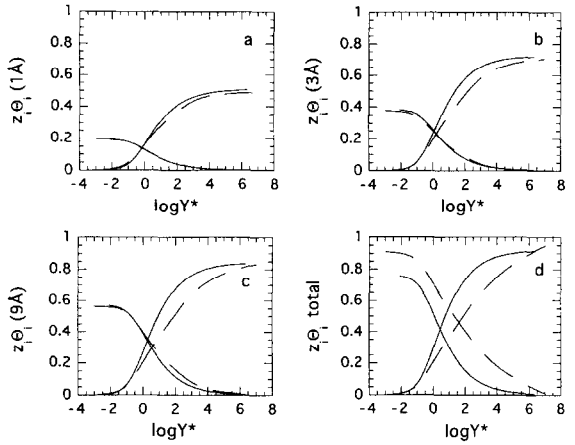

Fig. 6. The same as Fig. 3, but for a cylindrical surface. (Bulk monovalent ion concentration $n_{bl} = 10^{-3}$M.) Dashed lines, numerical P–B calculation; solid lines, approximate Eq. (38).

Just as in Fig. 3 for the plane, the accuracy of our approximate equations is high for short cut-offs, and gets worse but remains reasonable for longer cut-offs. In contrast to the planar case, the limiting values for the amounts bound are less than unity by the $(1 - 1/z_i\xi)$ factors. The rest of the charge is screened in the Debye–Hückel regime, i.e. each species participates in an amount proportional to its share of the bulk ionic strength. Since $I \approx n_{bl}$, almost all the residual charge is screened by the buffer counterions. This is reflected in the last panel of Fig. 6 for $z_i\Theta_i(\infty)$.

3. Influence of counterion sizes on competitive electrostatic binding

The above treatment assumed the counterions to be point charges. In this case only the polyion characteristics influence binding, through the quantity n_s. If competing species are of the same size, all the above conclusions are still valid, except that the distance of closest approach (ionic radius δ, Fig. 1) increases the effective radius of the polyion

$$R_{eff} = R + \delta \tag{40}$$

This, in turn, decreases the effective surface charge density

$$\sigma_{eff} = \sigma \frac{R}{R_{eff}} \tag{41}$$

Consequently, the total surface counterion concentration and thickness of the counterion layer should be rescaled as

$$n'_s = n_s \left(\frac{R}{R_{eff}} \right)^2 \text{ and } \lambda'_z = \lambda_z \frac{R_{eff}}{R} \tag{42}$$

For the sodium ion with hydrated radius $\delta_{Na} = 2.8$ Å near the B-DNA surface, $R_{eff} = 10 + 2.8 = 12.8$ Å, which yields $n'_s = 4.06$ M instead of 6.65 M and $\lambda'_{z=1} = 1.43$ Å instead of 1.19 Å for the point charge.

If the sizes of the competing counterions are different, and $\delta_1 < \delta_2$, the larger species will be at a disadvantage [20]. The surface will be considerably screened by the smaller ions before the larger ones can come into play. The measure of this effect is the value of the ion size difference $\Delta\delta = \delta_2 - \delta_1$ relative to the thickness of the screening layer of the smaller species $\lambda_{z=1} = \lambda$. We have assumed a monovalent buffer cation for concreteness.

If $\Delta\delta/\lambda < 1$, the ion competition is still very similar to that between point charges. For example, the power of the salt dependence of the binding constant S will still be z_2/z_1, but Y and K_{obs} will acquire the additional factor $e^{-z_2\Delta\delta/\lambda}$. This can also be viewed as a decrease in the apparent n_s such that one should use $n'^{z_2/z_1-1}_s = n^{z_2/z_1-1}_s e^{-z_2\Delta\delta/\lambda}$ instead of $n^{(z_2/z_1-1)}_s$ in expressions such as Eq. (28). Through this factor, the slight difference in the counterion sizes influences their competitive binding. In most cases, we do not know the exact size of the ligand, which introduces an uncertainty into our description. However, since $\Delta\delta/\lambda < 1$, the unknown factor $e^{-z_2\Delta\delta/\lambda}$ in Y or K_{obs} is on the order of unity. This defines the limit of accuracy in our prediction of the amount of bound ligand. The magnitude of $n^{(z_2/z_1-1)}_s$ for the particular pair of competing counterions can be found by fitting the experimental titration data to the P–B binding isotherm in Section 5 with respect to K_{obs}.

On the other hand, if $\Delta\delta/\lambda \gg 1$, the larger ligand "sees" a surface that is almost completely

screened. Therefore its binding is always weak (less than kT per ion) and depends weakly on the salt ($S_{\text{eff}} = 1$ instead of z_2/z_1) even if the ligand charge is very high.

Between these limits, when $\Delta\delta/\lambda \approx 1$, there should be intermediate behavior, in which the effective charge of the larger species is less than its actual value of z_2. This is because only the part of the ligand charge that is closer to the surface than

$$\delta_{\text{cr}} = \delta_1 + \lambda \tag{43}$$

participates in screening. Thus for Na^+ buffer, $\delta_{\text{cr}} = 2.8 + 1.4 = 4.2$ Å. The apparent power of the salt dependence of such binding is then $S_{\text{eff}} < S = z_2/z_1$.

If the ligand is a large globular particle with distributed charges, its effective binding charge z_{eff} (or S_{eff}) should be estimated with the numerical P–B procedure taking into account the specific geometry of the DNA–ligand complex. Nevertheless, we can use our analytical conclusions to obtain an estimate of this quantity

$$z_{\text{eff}} = \sum_{\delta_i < \delta_{\text{cr}}} z_i \, e^{-\Delta\delta_i/\lambda} \tag{44}$$

The summation is over all ligand charges that can approach closer than δ_{cr}, weighted with their reduction factors $e^{-\Delta\delta_i/\lambda}$. Therefore, titration data on strongly salt-dependent globular ligand binding should be fitted to the binding isotherm with both K_{obs} and z_2 as fitting parameters.

4. Typical calculations of competitive binding

In this section, we show how to use the theoretical formalism to answer some typical experimental questions related to competitive electrostatic binding. We begin with rough estimates of competing quantities of counterion species. We then consider more specific estimates of bound quantities within various distances from the polyion surface. This is an important issue in the analysis of experiments, since the definition of a "bound" ion varies from one technique to another. For example, NMR measures amounts bound within about 5 Å from the surface, gel electrophoresis measures the fraction of total screening charge bound strongly (with free energy per ion above $k_B T$) closer than r_d to the surface, and equilibrium dialysis measures the total amount affected by the polyion field, out to $r = \infty$. For pedagogical purposes, we use a question-and-answer format.

4.1. Rough estimates

Question: how much Mg^{2+} is needed to compete effectively with 0.5 M NaCl buffer?

Answer: here we need to determine not the exact Mg^{2+} concentration, but rather the order of magnitude that will provide comparable amounts of Mg^{2+} and Na^+ at the surface, such that $z_1\Theta_1/z_2\Theta_2 = 0.1$–$10$. This type of estimate is helpful for choosing the starting ligand concentration for a titration experiment, or choosing the lowest $[Mg^{2+}]$ that effectively replaces all Na^+ at the DNA surface. The very rough estimate $z_i\Theta_i = \tilde{n}_{si}$ together with Eq. (27) yields $Y \approx 1$. The value of n_s, taking into account the size of Na^+, is approximately 4 M. Differences in the counterion sizes can further reduce the effective n_s. At the level of accuracy required here, we can use just the order of magnitude $n_s \approx 1$ M. This yields a simple relationship that could often be used for rough estimates like the present one

$$n_{b2} \sim n_{b1}^{z_2/z_2} \tag{45}$$

Therefore $n_{\text{Mg}} \approx n_{\text{Na}}^2 = 0.25$ M.

Question: how much Mg^{2+} will we need in fifty-fold-diluted buffer?

Answer: according to Eq. (45), the Mg^{2+} concentration should be reduced $50^2 = 2500$ times.

Question: how much spermidine^{3+} (Spd^{3+}) competes effectively with 10 mM NaCl?

Answer: according to the approximate Eq. (45), $n_{\text{Spd}} \approx (n_{\text{Na}})^3 = 1$ μM.

Question: how much Spd^{3+} will we need in fiftyfold-diluted buffer?

Answer: according to Eq. (45), $[Spd^{3+}]$ should be reduced $50^3 = 125\,000$ times!

In general, it follows from Eq. (28) that to maintain any particular degree of binding while varying the bulk composition, one should keep $n_{b2}/n_{b1}^{z_2/z_1}$ constant. If $z_2/z_1 > 1$, a variation in the ionic strength (which is usually approximately n_{b1}), requires a much larger change in the ligand concentration.

4.2. More precise estimates with various criteria of "binding"

4.2.1. High salt: 0.1 < I < 1 M (planar geometry)

Question: how much total Mg^{2+} is bound to B-DNA if the bulk solution contains 0.2 M sodium buffer and 10 mM $MgCl_2$?

Answer: $I \approx 0.2$ M is a high enough ionic strength for the effects of polyion cylindricality not to have to be considered. We can then use the formulas for planar geometry. From Eq. (28) we see that $Y = 0.01/(0.2)^2 \times 4 \approx 1$. We plot $Y = \tilde{n}_{s2}/(1-\tilde{n}_{s2})^2$ according to Eq. (27), and read from the graph the values corresponding to $Y = 1$: $\tilde{n}_{s1} \approx 0.62$, $\tilde{n}_{s2} \approx 0.38$. We calculate the total amounts of charge neutralization with Eq. (32) and (33), finding $\nu_1(\tilde{n}_{s2}) = 1.18$, $\nu_2(\tilde{n}_{s2}) = 0.71$, $z_1\Theta_1(\infty) = 0.62 \times 1.18 = 0.73$, and $z_2\Theta_2(\infty) = 0.38 \times 0.71 = 0.27$. Since the ionic strength in this case is rather high, the accuracy of this estimate is limited by the amount of screening charge residing in the Debye–Hückel tail. According to Eq. (31), $\mathrm{err}_1 \approx (I/n_s)1/2 \approx (0.22/4)^{1/2} = 0.23$.

Question: how can we account for the diffuse Debye–Hückel screening?

Answer: the total amounts calculated as bound in the preceding paragraph are the amounts within the cut-off $r_{cut} = r_d$, which are the $z_i\Theta_i(\infty)$ multiplied by the corresponding $g(r_d/\lambda_{zi})$ factors from Eq. (13). In this particular case, $r_d = 6.6$ Å, $\lambda_{z1} = 1.43$ Å, and $\lambda_{z2} = 0.71$, so $g_1 = 0.70$ and $g_2 = 0.82$. This yields $z_1\Theta_1(r_d) = 0.73 \times 0.70 = 0.51$ and $z_2\Theta_2(r_d) = 0.27 \times 0.82 = 0.22$. The residual fractional charge, approximately 0.27, is weakly (less than k_BT per ion) bound beyond r_d and is almost all Na^+.

Question: how can we calculate binding close to the surface, as in NMR experiments?

Answer: NMR measures ionic concentrations within about 5 Å from the DNA surface. Disregarding the difference in Na^+ and Mg^{+2} ion sizes for the simplest estimate, we calculate the cut-off distance $r_{cut} = 5 - 2.8 = 2.2$ Å for the distance of closest approach of the sodium ion with $\delta = 2.8$ Å. The corresponding $g(2.2\ \text{Å}/\lambda_{zi})$ factors are 0.43 for Na^+ and 0.66 for Mg^{2+}. Therefore the amounts bound are $z_1\Theta_1(2.2\ \text{Å}) = \tilde{n}_{s1}g_1 = 0.62 \times 0.43 = 0.27$, and $z_2\Theta_2(2.2\ \text{Å}) = \tilde{n}_{s2}g_2 = 0.38 \times 0.66 = 0.25$. At such short cut-offs near λ_z, the g-factors are highly sensitive to the value of r_{cut}, but they saturate very quickly at $r_{cut} \approx 10\lambda_z \approx 8$ for $z = 2$.

4.2.2. Low salt: I < 0.1 M (cylindrical geometry)

Question: how much total Spd^{3+} is bound to B-DNA if the solution contains 10 mM sodium buffer and 4 μM Spd^{3+}?

Answer: $I \approx 0.01$ M is the range of ionic strength where the cylindrical curvature of the DNA becomes important. We first use Eq. (28) and (37) to calculate $Y^* = Y\chi = (n_{Spd}n_{s2}/n_{Na}^3) \times 0.23 = 14.7$. We obtain a plot of $\tilde{n}_{s2}/(1-\tilde{n}_{s2})^3$ vs. Y^*, and read from it the values of $\tilde{n}_{s1} = 0.35$ and $\tilde{n}_{s2} = 0.65$ corresponding to $Y^* = 14.7$. The total amounts of charge due to each species are then calculated with Eq. (39). The "strongly bound" fractions of charge due to each species, bound with more than kT per ion of binding free energy within r_d, are $z_2\Theta_2(\infty) = \tilde{n}_{s2}(1 - 1/z_2\xi)\nu_2 = 0.65 \times 0.92 \times 0.81 = 0.49$, and $z_1\Theta_1(\infty) = \tilde{n}_{s1}(1 - 1/z_1\xi)\nu_1 = 0.35 \times 0.76 \times 1.35 = 0.36$. The accuracy of this estimate is approximately $\sqrt{I/n_s} = 0.05$. The rest of the charge, $1 - (z_1\Theta_1 + z_2\Theta_2) = 0.15$, is screened by the Na^+ dominating in the bulk solution within the weakly bound Debye–Hückel tail.

Question: how much of each ion is bound within 3 Å of the surface?

Answer: the fractions of neutralizing charge bound within 3 Å from the surface are $z_2\Theta_2(3\ \text{Å}) = \tilde{n}_{s2}\,g(3/\lambda^*_{z2})(1 - 1/z_2\xi) = 0.65 \times 0.74 \times 0.92 = 0.44$ and $z_1\Theta_1(3\ \text{Å}) = \tilde{n}_{s1}\,g(3/\lambda^*_{z1})(1 - 1/z_1\xi) = 0.35 \times 0.44 \times 0.76 = 0.12$. Here we used Eq. (22) to calculate that $\lambda^*_{z1} = \lambda_{z1}/(1 - 1/z_1\xi) = 1.88$ Å and $\lambda^*_{z2} = 0.52$ Å. These estimates should be fairly accurate, given that the cut-off distance is known well enough.

4.3. Influence of the dielectric constant of the solution on binding

Question: how should the Spd^{3+} concentration change to maintain the same degree of binding to DNA in sodium buffer if 40% ethanol by volume is added?

Answer: 40% (v/v) ethanol lowers the dielectric constant of the solution to $\varepsilon' = 60$ compared with 80 for pure water. This increases the total surface coun-

Table 1
Binding isotherms and apparent association constants for ligands of charge z_2 in buffer of counterion valence z_1 in planar (high salt) and cylindrical (low salt) regimes

Planar	Cylindrical
$\frac{\Theta_2}{n_{b2}} = K_{obs}(1-\frac{z_2\Theta_2}{\eta})^{z_2/z_1}$	$\frac{\Theta_2}{n_{b2}} = K^*_{obs}(1-\frac{z_2\Theta_2}{\eta})^{z_2/z_1}$
$K_{obs} = \frac{n_s^{z_2/z_1}-1}{n_{b1}^{z_2/z_1}z_2}\eta$	$K^*_{obs} = K_{obs}\chi$,
	$\chi = \left[\frac{(1-1/z_1\xi)^{z_2/z_1}}{1-1/z_2\xi}\right]^2$
$\eta = g(\frac{r_{cut}}{\lambda_{z2}})$	
for $r_{cut} < r_d$	$\eta = g(\frac{r_{cut}}{\lambda^*_{z2}})(1-1/z_2\xi)$ for $r_{cut} < r_d$
$\eta = \nu_2$ for total binding $\Theta_2(\infty)$	$\eta = \nu_2(1-1/z_2\xi)$ for total binding $\Theta_2(\infty)$

terion concentration n_s by the factor $\varepsilon/\varepsilon' = 80/60$. Since Y should be constant to maintain the same degree of binding, Eq. (28), the Spd^{3+} concentration should be lowered proportionally to $n_s^{z_2/z_1-1}$, $(\varepsilon/\varepsilon')^2 = 1.8$. The apparent electrostatic binding constant of Spd^{3+} will increase by the same factor. This calculation assumes, of course, that water and alcohol mix to form a uniform solvent with no preferential hydration or other specific effects.

5. Analysis of competitive binding isotherms

5.1. Analytical P–B isotherm for two counterion species

The relationships we have given above are sufficient to write out the explicit expression for the binding isotherm for electrostatic binding of a charged ligand (species 2) in a given buffer (species 1). The exact results are summarized in Table 1. However, for most practical purposes it is more appropriate to use the simplified form of the binding isotherm

$$\frac{\Theta_2}{n_{b2}} = K_{obs}(1-z_2\Theta_2)^{z_2/z_1} \quad (46)$$

which uses the approximation $z_2\Theta_2 = \tilde{n}_{s2}$. It assumes the correction factor $\nu_2 = 1$, and neglects the $1/(1-1/z_2\xi)$ factor multiplying $z_2\Theta_2$ in the equation for the cylindrical regime. The latter makes little difference for the shape of the Scatchard plot, but allows fitting of the binding data to a single expression over a wide range of salt concentration. Variation of ν_2 with the amount of ligand bound is essential only for high degrees of binding, $z_2\theta_2 \approx 1$, where the ratio Θ_2/n_{b2} is so small that its variation is insignificant for the shape of the Scatchard plot.

The apparent binding constant in Eq. (46) then equals

$$K_{obs} = \frac{(n'_s)^{z_2/z_1-1}}{n_{b1}^{z_2/z_1}z_2} \quad (47)$$

The main part of the salt dependence of K_{obs} is contained in the $n_{b1}^{-z_2/z_1}$ factor, yielding the conventional value z_2/z_1 for the slope S, Eq. (3), and a new expression for the dependence of K_{obs} on the system parameters through n'_s. This is proportional to n_s, Eq. (11), but can differ from it by a size factor of order unity, Eq. (42). If not for this uncertainty, Eq. (46) and (47) would completely describe the binding. We can still approximately predict binding behavior by assuming $n'_s \approx 1$–6 M. However, if titration data are available they should be fitted to Eq. (46) to obtain K_{obs} at several ionic strengths.

The factor γ in Eq. (47) varies from its cylindrical value of χ (Eq. (37)) in low salt, $I \ll n'_s/4\xi^2 \approx 0.1$ M, to its planar value of unity in the range $n'_s/4\xi^2 < n'_s$. For point charges with $n'_s = n_s = 6.6$ M, this range is 0.1 M $\leq I \leq$ 1 M. This growth of γ reflects the slight increase of counterion accumulation near the cylindrical macroion with increasing solution ionic strength upon the transition from cylindrical to planar regimes. It results in slower growth of K_{obs} with decreasing salt, relative to the conventional $n_{b1}^{-z_2/z_1}$ dependence. This is one possible origin of the experimental observation [29] that S is usually somewhat smaller than z_2/z_1, another being the large size of the ligand.

The slope S decreases to unity when $I > n'_s$. This reflects a transition to a completely different binding regime [19], in which the P–B equation becomes linear and r_d becomes smaller than λ_z. The salt-in-

dependent ionic surface layer then is replaced by a Debye–Hückel exponential distribution. The relative amounts of neutralizing species in this case are the same as their contributions to the ionic strength

$$z_i\Theta_i = z_i^2 n_{bi}/I \tag{48}$$

This yields a weak binding constant $K_{obs} \approx 1$ ($G_{bind}/kT < 1$) which depends linearly on the salt concentration.

5.2. Binding of spermidine^{3+} to B-DNA

The analytical approach described above is suitable for the analysis of equilibrium dialysis data [8] on Spd^{3+} binding to DNA in buffer with Na^+ as the cation. Fig. 7 shows various representations of the data and the theoretical treatment, along with the numerical P–B results. Panel a shows Scatchard plots for three salt concentrations, with data points fitted by the conventional McGhee–Von Hippel isotherm, Eq. (4) and by the P–B isotherm, Eq. (46). The two fits are rather similar, the latter being somewhat steeper. The parameters of these fits, and on data for two other NaCl concentrations, are given in Table 2. We see that K_{obs} values from the P–B fits are only slightly larger. The data are fitted somewhat better with Eq. (4), which has both K_{obs} and N as fitting parameters. However, this "improved" fitting to the physically questionable "site size" can bias estimates of the physically significant quantity K_{obs}. Indeed, as seen from Table 2, the apparent N obtained in such fitting varies randomly with ionic strength, which clearly comes from the scatter of the experimental points rather than any physical trend.

Log–log plots of K_{obs} vs. n_{b1}, Fig. 7b, give similar average slopes S somewhat lower than $z_2/z_1 = 3$: 2.44 for P–B and 2.68 for McGhee–von Hippel. Intercepts on the log n_{b1} axis are close to zero in both cases, meaning that the effective surface concentration n_s' is close to 1 M.

An analysis in Fig. 7c of S values obtained from the P–B theory shows the expected magnitude close to $z_2/z_1 = 3$ at the low end of the experimentally studied salt range, $n_{b1}v \approx 0.05$ M. The slope S decreases strongly with increasing salt concentration, and reaches a value of approximately 1.7 at the high end, $n_{b1} \approx 0.16$ M. This is consistent with the predicted slope decrease within the transition salt concentration range, which in the case of $n_s' = 1$ M is 0.02 M $< I <$ 0.2 M. The strong scattering of S values obtained from the McGhee–von Hippel analysis is a consequence of the inconsistency of the "site size" variation.

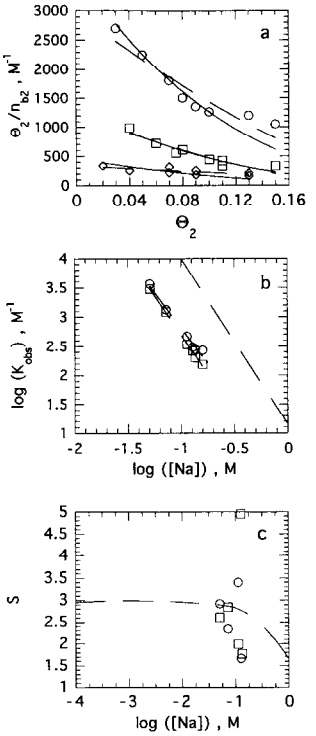

Fig. 7. (a) Scatchard plots for equilibrium dialysis data on Spd^{3+} binding to B-DNA (calf thymus or T7) in sodium buffer [8] at (○) $n_{b1} = 0.051$ M, (□) $n_{b1} = 0.072$ M, and (◇) $n_{b1} = 0.113$ M. Data are fit to the McGhee–von Hippel (dashed line) and analytical P–B (solid line) binding isotherms. The fitting parameters for these three buffer concentrations and three other ones are listed in Table 2. (b) Plot of $\log(K_{obs})$ vs. $\log[Na^+]$ from Table 2 for Spd^{3+}–DNA binding. (○) Analytical P–B parameters, $\log K_{P-B,obs} = -2.44\log[Na] + 0.37$; (□) McGhee–von Hippel parameters, $\log K_{MGvH,obs} = -2.68\log[Na] + 0.01$. Dashed line, numerical P–B calculation for point charge ions, $\log K_{P-Bnum,obs} = -2.93\log[Na] + 1.11$. (c) Negative derivative of the plot in panel (b), giving $S = -d\log K_{obs}/d\log n_{b1}$. The symbols are the same as in (b).

The values of S in Fig. 7c obtained from the full numerical solution to the P–B equation behave similarly to the experimental values. The main differences are that the numerical S starts to deviate from 3 at somewhat higher salt concentration, and falls

Table 2
Fitting parameters for the binding of spermidine^{3+} to B-DNA at the indicated NaCl molarities, according to analytical P–B ($K_{obs\ P-B}$) and McGhee–von Hippel ($K_{obs\ MG-vH}$, N) theories [a]

n_{bl} (M)	$K_{obs\ P-B}$ (M^{-1})	$K_{obs\ MG-vH}$ (M^{-1})	N
0.051	3682±170	2981±225	3.34±0.30
0.072	1344±53	1213±116	3.94±0.34
0.113	469±48	337±40	2.41±0.55
0.128	307±13	263±17	3.40±0.38
0.135	281±24	202±9	2.64±0.20
0.158	271±53	153±20	2.08±0.32

[a] Data from Braunlin et al. [8].

less abruptly. This is due to the higher n_s value, 6.6 M for point charges, used for the numerical calculations as opposed to the $n'_s \approx 1$ M that best fits experiment. This also accounts for the larger intercept of the numerical calculation in Fig. 7b.

In Fig. 7a, the P–B curves are slightly steeper than the experimental points, a trend that is more pronounced in higher salt concentration. The reason for this, in our theory, is the transition from cylindrical to planar non-linear screening and then to linear screening with increasing salt concentration. Calculations of this effect on the shape of the Scatchard plot are shown in Fig. 8. Increasing the ionic strength results in a slightly smaller slope, which eventually drops to unity at $I > 1$ M. Thus the simple picture of a fixed stoichiometry of ion exchange should hold rather well for low ionic strengths. However, this apparent stoichiometry decreases due to screening at higher salt.

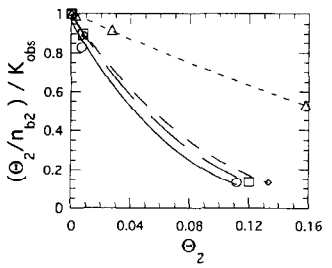

Fig. 8. Scatchard plots constructed from numerical P–B calculations for point trivalent cations binding to B-DNA in the presence of point monovalent competitors at concentrations, from bottom to top, of 10^{-4}, 10^{-2}, 10^{-1}, and 10 M. All curves are normalized by the appropriate K_{obs}.

6. Competitive binding of several counterion species

The competition of more than two types of counterions is often of interest. The equations of Section 2 can easily be extended for an arbitrary number of counterion species. The equivalents of Eq. (25) and (26), together with the basic approximation $z_i\Theta_i = \tilde{n}_{si}$, yield equations that completely describe the competition between multiple species

$$\sum_i z_i\Theta_i = 1 \tag{49}$$

and

$$\left(\frac{z_i\Theta_i n_s}{n_{bi}}\right)^{1/z_i} = \left(\frac{z_j\Theta_j n_s}{n_{bj}}\right)^{1/z_j} \tag{50}$$

For example, the binding isotherm for each species can be written in the form

$$\frac{\Theta_i}{n_{bi}} = k_{ij}\left(1 - \sum_{k\neq j}^{\infty} z_k\Theta_k\right)^{z_i/z_j} \tag{51}$$

where

$$K_{ij} = \frac{n_s'^{(z_i/z_j-1)}}{z_i n_{bj}^{z_i/z_j}}\gamma_{ij} \tag{52}$$

is the binding constant of the ith species due to its competition with the jth species. Eq. (52) is fully analogous to Eq. (47) for two-counterion competition, with the same transition in the expression for γ between low and high salt concentrations. Eq. (51) should be compared to the analogous McGhee–von Hippel expression

$$\frac{\Theta_i}{n_{bi}} = K_i\frac{\left(1 - \sum_j N_j\Theta_j\right)^{N_i}}{\left(1 - \sum_j (N_j - 1)\Theta_j\right)^{N_i - 1}} \tag{53}$$

Again, the P–B expression lacks the site exclusion term and does not treat the site size as a variable. It also describes competition not only in the monovalent salt concentration, but deals with all counterion species on the same basis, thus introducing the binding constant K_{ij} for the competition of any two counterion species.

A common experimental situation has three types of counterions. One is the buffer counterion, typically Na^+ or K^+, and the others are higher valent ligands, one of which is labeled. Monitoring the binding of the labeled species in the course of a titration with the unlabeled one, followed by fitting the data to a presumed isotherm, enables the determination of the binding constant of the unlabeled counterion if the binding constant of the labeled one is known under the same buffer conditions. An example is the competition between spermine^{4+} (Spe^{4+}) and spermidine^{3+} (Spd^{3+}) [8] shown in Fig. 9. The [Na] = 0.127 M and $[Spe^{4+}] = 1.16 \times 10^{-4}$ M were fixed, while the $[Spd^{3+}]$ was varied. The binding constants obtained in this indirect way using Eq. (53) were similar to those obtained from direct binding experiments without the competing ligand, and had similar strong salt concentration dependence.

We have fitted the same points using our theoretical approach, embodied in an isotherm derived from Eq. (51) and (52) but rearranged to relate the amount of ith species bound to the binding constants of all other participating ligands

$$\frac{\Theta_i}{n_{bi}} = K_{ij}\left(1 - z_i\Theta_i - \sum_{k\neq i,j}(z_i\Theta_i)^{z_k/z_i}K_{ki}z_k n_{bk}\right)^{z_i/z_j} \quad (54)$$

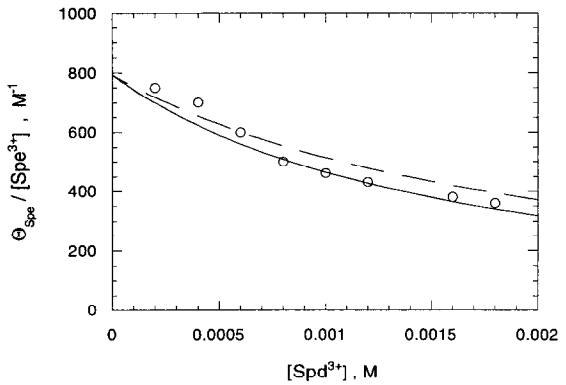

Fig. 9. Competition of spermidine (Spd^{3+}) with 1.16×10^{-4} M spermine (Spe^{4+}) in a background of 0.127 M Na^+ buffer [8], fitted according to Eq. (55) with $n'_s = 2$ M (solid line) and $n'_s = 6$ M (dashed line).

Under the particular experimental conditions, this takes the form

$$\frac{\Theta_{Spe}}{1.16\times10^4} = \frac{1}{4}\left[\frac{(n'_s)_{Spe,Na}}{0.127^4}\right] \times\left[1 - 4\Theta_{Spe} - \left(\frac{4\Theta_{Spe}}{1.16\times10^{-4}}\right)^{3/4} \times(n'_s)^{-1/4}_{Spe,Spd}\, n_{Spd}\right]^4 \quad (55)$$

Calculations were performed for $n'_s = 2$ M and 6 M. Both fit the data fairly well; the differences in the curves illustrate the sensitivity to the fundamental surface binding parameter.

7. Conclusions

We have described a tractable analytical approach, based on the non-linear Poisson–Boltzmann equation, to competitive counterion binding to highly charged polyions such as DNA. Our treatment in this paper summarizes and extends our previous work [19,20]. Tests of this approach against numerical solutions of the P–B equation and experimental data indicate that it provides an adequate account of non-specific electrostatic binding of charged ligands to polyelectrolytes. It self-consistently reproduces the major features of such binding, especially the anti-cooperativity and strong salt dependence. Both features are defined by the ratio of charges of the competing species. Anti-cooperativity occurs even for point charges, and does not require steric repulsion between the ligands. In fact, steric effects in purely electrostatic binding are minimal even for ligands as large as 10–15 Å due to the strong electrostatic repulsion between them within the thin surface screening layer. A similar observation was made by Ray and Manning [18] in the context of counterion condensation theory.

The P–B approach yields, without prior assumptions of fixed stoichiometry, the familiar low-salt

ion-exchange behavior embodied in Eq. (1), which occurs because a majority of the screening counterions reside in the very thin surface layer, independent of bulk salt. The parameters of this surface layer start to change slowly with increasing salt for $I > n_s'/\xi^2 \approx 0.1$ M. The weak additional charge accumulation in this range leads to a decrease in polyion–ligand "ion pairs", and thus in the power S of the salt concentration dependence of the binding constant. At even higher salt concentration, $I \geq 1$ M, S drops to about 1, manifesting the complete breakdown of the ion-exchange picture. Thus the P–B approach explains naturally the observed variation of S over the entire range of ionic strength. Truly linear $\log(K_{obs})$ vs. log[salt] behavior with constant S and intercept near 1 M is typical only for sufficiently low salt concentrations. The range of I where S starts to decrease from its maximum value depends on the polyion surface charge density. It is usually about 0.1 M for double-stranded DNA, and somewhat less for single-stranded polynucleotides.

The analytical P–B treatment gives us a theoretical expression for electrostatic binding constants, and allows us to estimate the amounts of competing species bound within an arbitrary distance from the polyion surface. The accuracy of the estimate is comparable to that from numerical P–B calculations, while replacing the complex numerical calculations with algebraic equations similar in ease of application to those of the counterion condensation theory [15]. The prediction of the amounts bound can be carried out with modest uncertainty, which comes largely from the imprecisely known effective sizes of the competing counterion species. Moderate differences $\Delta\delta$ in the counterion sizes, less than the surface layer thickness $\lambda \approx 1$–1.5 Å, appear only as a factor $e^{-z_2\Delta\delta/\lambda}$ in Y and K_{obs}. A larger difference in ion sizes will also affect the effective charge of the ligand z_{eff} in competitive electrostatic binding, so that it may be different from the total charge z_2. For small ions with well-defined charges, fits of experimental titration data to the isotherm Eq. (46) can be carried out with K_{obs} as the only variable parameter. For larger ions, both K_{obs} and z_2 should be treated as adjustable parameters. The tests for self-consistency of such fitting should be that $S \approx z_{eff}$, and that n_s' obtained from K_{obs} should be in the range 0.5–5 M for B-DNA.

Our treatment of the purely electrostatic binding of relatively simple ligands does not, of course, take into account many of the complexities encountered in DNA–ligand binding. These include non-electrostatic contributions which will often have a significant enthalpic component, changes in hydration of the binding partners, and charge localization in globular proteins [30–33]. However, despite these complexities, a surprising number of charged ligands bind to polyions in a distinctly electrostatic fashion. Our approach provides a useful way to characterize and quantify this type of binding behavior.

References

[1] M.T. Record, Jr., C.F. Anderson and T.M. Lohman, Q. Rev. Biophys., 11 (1978) 103.
[2] J.D. McGhee and P.H. von Hippel, J. Mol. Biol., 86 (1974) 469.
[3] W.H. Braunlin, C.F. Anderson and M.T. Record, Jr., Biopolymers, 25 (1986) 205.
[4] W.H. Braunlin, C.F. Anderson and M.T. Record, Jr., Biochemistry, 26 (1987) 7724.
[5] W.H. Braunlin, T. Drakenberg and L. Nordenskiöld, Biopolymers, 26 (1987) 1047.
[6] W.H. Braunlin, T. Drakenberg and L. Nordenskiöld, J. Biomol. Struct. Dyn., 10 (1992) 333.
[7] W.H. Braunlin and Q. Xu, Biopolymers, 32 (1992) 1703.
[8] W.H. Braunlin, T.J. Strick and M.T. Record, Jr., Biopolymers, 21 (1982) 1301.
[9] M.D. Frank-Kamenetskii, V.V. Anshelevich and A.V. Lukashin, Sov. Phys. Usp., 151 (1987) 595.
[10] M. Guéron and G. Weisbuch, Biopolymers, 19 (1980) 353.
[11] M. Le Bret and B.H. Zimm, Biopolymers, 23 (1984) 271.
[12] M. Le Bret and B.H. Zimm, Biopolymers, 23 (1984) 287.
[13] G.R. Pack and G. Lamm, Int. J. Quantum Chem.: Quantum Biol. Symp., 20 (1993) 213.
[14] G. Lamm, L. Wong and G. Pack, Biopolymers, 34 (1994) 227.
[15] G.S. Manning, Q. Rev. Biophys., 11 (1978) 179.
[16] G.R. Pack, G.A. Garrett, L. Wong and G. Lamm, Biophys. J., 65 (1993) 1363.
[17] I. Rouzina and V.A. Bloomfield, J. Phys. Chem., 100 (1996) 1977.
[18] J. Ray and G.S. Manning, Biopolymers, 32 (1992) 541.
[19] I. Rouzina and V.A. Bloomfield, J. Phys. Chem., 100 (1996) 4292.
[20] I. Rouzina and V.A. Bloomfield, J. Phys. Chem., 100 (1996) 4305.
[21] T. Alfrey, Jr., P.W. Berg and H. Morawetz, J. Polym. Sci., 7 (1951) 543.
[22] R.M. Fuoss, A. Katchalsky and S. Lifson, Proc. Natl. Acad. Sci. USA, 37 (1951) 579.

[23] D. Stigter, J. Colloid Interface Sci., 53 (1975) 296.
[24] M. Fixman, J. Chem. Phys., 70 (1979) 4995.
[25] B.H. Zimm and M. Le Bret, J. Biomolec. Struct. Dyn., 1 (1983) 461.
[26] M. Guéron and G. Weisbuch, Biochimie, 63 (1981) 821.
[27] M. Guéron and J.-P. Demaret, J. Phys. Chem., 96 (1992) 7816.
[28] R.J. Bacquet and P.J. Rossky, J. Phys. Chem., 92 (1988) 3604.
[29] M.T. Record, Jr., T.M. Lohman and P.L. de Haseth, J. Mol. Biol., 107 (1976) 145.
[30] K.A. Sharp and B. Honig, J. Phys. Chem., 94 (1990) 7684.
[31] V. Misra, K. Sharp, R. Friedman and B. Honig, J. Mol. Biol., 238 (1994) 245.
[32] V. Misra, J. Hecht, K. Sharp, R. Friedman and B. Honig, J. Mol. Biol., 238 (1994) 264.
[33] V.K. Misra and B. Honig, Proc. Natl. Acad. Sci. USA, 92 (1995) 4691.